CrystEngComm

PAPER

View Article Online
View Journal | View Issue

Cite this: *CrystEngComm*, 2022, **24**, 2336

Crystal engineering of aurophilic supramolecular architectures and coordination polymers based on butterfly-like copper–dicyanoaurate complexes: vapochromism, *P–T* behaviour and multi-metallic cocrystal formation†

Emanuele Priola, ‡*[a] Nadia Curetti,‡[b] Domenica Marabello,‡[a] Jacopo Andreo, [c] Alessia Giordana, [a] Luca Andreo, [a] Piera Benna, ‡[b] Paulo Tarso Cavalcante Freire, [d] Paola Benzi,‡[a] Lorenza Operti‡[a] and Eliano Diana ‡*[a]

Received 23rd July 2021,
Accepted 17th February 2022

DOI: 10.1039/d1ce00964h

rsc.li/crystengcomm

Using the equilibrium properties of the Cu(II) cation in the presence of chelating ligands and the characteristics of the dicyanoaurate anion, we were able to obtain a family of 5 bimetallic Cu–Au compounds with supramolecular architectures based on aurophilic interactions. These compounds have been tested for vapochromism at different temperatures and pressures. One of the obtained products shows reversible vapochromism in the presence of ammonia and the process has been studied using IR and UV-vis absorption spectroscopy. The behaviour at variable temperatures and pressures of these crystalline materials has been investigated, showing the effect of these two variables. Moreover, an isosymmetric phase transition at 1.2 GPa has been detected and studied with Raman and SC-XRD. Finally, Cu–Au molecular building blocks have been used to construct cocrystals, opening the way for the crystal engineering of new multimetallic compounds based on aurophilic interactions.

Introduction

During the last few decades, dicyanoaurate has proven to be a good metalloligand and an interesting tecton for building supramolecular networks based on strong coordinative bonds and weak aurophilic interactions.[1–3] The great stability of this complex ($\log(\beta_{form})$ = 37 at 25 °C)[4–6] ($\beta_{form} = K_1K_2$, K_n = formation constant of ML_n) makes it possible to manipulate it in several chemical environments (for example, in the presence of acids or competing ligands) and the low steric hindrance favours the formation of Au(I)···Au(I) contacts despite the anionic nature.[7–10] At the same time, the linearity and ambidentate bridging coordination mode have been used to build coordination networks that are often an expanded version of cyanide-derived compounds (*e.g.* expanded Prussian blue analogues, Hoffman-like frameworks and super-perovskites).[11–13] These materials can show interesting properties such as: vapochromism, photoluminescence at room temperature, high birefringence, and non-classical responses to temperature and pressure.[14–27] However, a systematic investigation of dicyanoaurate-based bimetallic molecular complexes that aggregate only by means of aurophilic interactions has not yet been performed, although the study of molecular gold strings of other gold(I) complexes is well developed.[28] In a previous publication, we reported a series of molecular complexes of Zn(II) with these characteristics, and we demonstrated their preformation in solution at concentrations where no aurophilic interactions are present.[29] The formation of $\{(L)_2Zn[Au(CN)_2]\}^+$ (L = chelating ligand) is favoured with respect to $[Zn(L)_3]^+$ due to the great difference between K_2 and K_3 formation constants for Zn(II) complexes (see Fig. 1 for 2,2′-bipyridine and 1,10-phenanthroline).[30] This is mainly due to the absence of crystal field stabilisation and the small ionic radius of this cation.[31,32] In this paper we focus our attention on copper–

[a] *Department of Chemistry, Università di Torino, Via Pietro Giuria 7, 10125 Torino, Italy. E-mail: emanuele.priola@unito.it, eliano.diana@unito.it*
[b] *Department of Earth Sciences, Università di Torino, Via Valperga Caluso 35, 10125 Torino, Italy*
[c] *BCMaterials, Basque Center for Materials, UPV/EHU Science Park, 48940 Leioa, Spain*
[d] *Departamento de Física, Universidade Federal do Ceará, C.P. 6030, Campus do Pici, 60455-760, Fortaleza, CE, Brazil*

† Electronic supplementary information (ESI) available. CCDC 2078267, 2078268, 2078273, 2078274, 2078276, 2078280, 2078281–2078285 and 2078286–2078289. For ESI and crystallographic data in CIF or other electronic format see DOI: 10.1039/d1ce00964h

‡ CriSDi, Interdepartmental Center for Crystallography, Via Pietro Giuria 7, 10125, Torino, Italy.

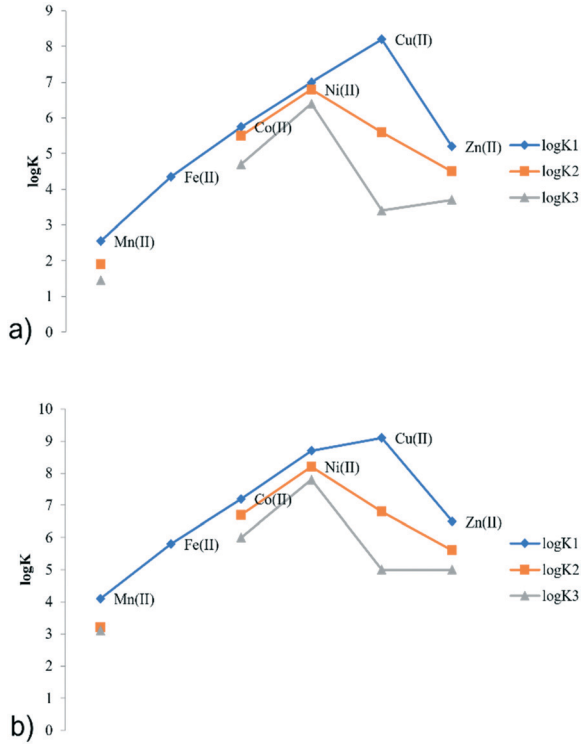

Fig. 1 Log K_1, log K_2 and log K_3 coordination constants for 2,2′-bipyridine (a) and 1,10-phenanthroline (b) with the late 1st transition metals in the +2 oxidation state.

dicyanoaurate bimetallic complexes in the presence of chelating ligands. The Cu(II) ion is a good candidate for the formation of bis-chelated species, as a consequence of the Jahn–Teller effect (or pseudo Jahn–Teller for heteroleptic complexes) which destabilises the tris-chelated form and generates systems with $K_2 \gg K_3$ (see Fig. 1).[30] From a structural point of view, in complexes the Jahn–Teller effect causes: (i) with 2,2′-bipyridine-like ligands, an out-of-plane distortion of one chelating ligand and (ii) with the more rigid phenanthroline, a shift of one of the ligands around the metal centre (see Fig. S1 and S2 in the ESI†).[33–36] Moreover, the previously described copper–dicyanoaurate materials have shown very promising vapochromism (modification of electronic absorption or emission spectra in the presence of specific chemical species in the atmosphere) and anomalous pressure–temperature (*P*–*T*) behaviour.[17,37–39]

In this paper, we report the synthesis and characterization of a family of 5 new bimetallic complexes (see Table 1) obtained using four nitrogen donor chelating ligands (L1 = 2,2′-bipyridine; L2 = 1,10-phenanthroline; L3 = 1-(2-pyridy)-3-(4-trifluoromethylphenyl)imidazo[1,5-*a*]-pyridine and L4 = 2-(2′-pyridyl)-1,8-naphthyridine, see Fig. 2). These ligands were chosen for their differences in shape, steric hindrance, rigidity, coordination ability and electronic properties. From a synthetic point of view, in the literature it is reported that in the presence of chelating nitrogen donor and cyanide ligands, both Cu(II) and Cu(I) products can be obtained independently from the starting oxidation state.[40–44] The vapochromic behaviour was checked for all the synthesized materials toward common solvent vapours and ammonia. Crystals of compound **1** can be considered prototypical for aurophilic-based supramolecular bimetallic architectures and were studied at variable temperatures and pressures. This crystallographic study rationalizes the effect of non-environmental conditions on these supramolecular networks. Finally, considering the stability and permanence of these bimetallic complexes in solution, we decided to use them as building blocks in more complex architectures with other d^{10} metal centres, obtaining cocrystals and heteroleptic complexes.

Experimental

Materials and general methods

All reagents have been obtained from Sigma-Aldrich, except for ligands L3 and L4 which were synthesised according to literature procedures.[45–47] No further purification was performed on the commercial reagents. Regarding the metal source, we report here the copper salt that achieved the best yield and purity of the final compound, but it is worth noticing that all reactions can be carried out with copper oxo salts or copper chloride, similarly to that observed in the preparation of Zn(II)–dicyanoaurate compounds.[29] Correspondence between the bulk and SC-XRD structures, as well as sample purity, was verified for compounds **1–6** through elemental analysis (C, H, N and S) carried out using a Thermo Flash EA 1112 CHNS-O analyser. When a mixture of more than one compound has been obtained, elemental analysis was not possible, but Raman and IR spectroscopic characterization has been performed. For all the synthesised compounds **1–6** the entire IR and Raman spectra can be found in the ESI.†

Synthesis

(1) {Cu(L1)$_2$[(μ-CN)Au(CN)]}[Au(CN)$_2$]. 43.3 mg of $Cu(SO_4)\cdot 5H_2O$ and 54.0 mg of L1 were dissolved in 10 ml of 50 : 50 EtOH/H_2O, and a separate solution in the same solvent

Table 1 Au–Cu bimetallic new products reported in this paper. For the structural formula of complexes **1–6** see Scheme S1 in the ESI†

Compound	Aurophilic interactions	Dimensionality	Coordination polyhedron of Cu sites
(**1**) {Cu(L1)$_2$[(μ-CN)Au(CN)]}[Au(CN)$_2$]	Yes	1D supramolecular chain	Trigonal bipyramid
(**2**) {Cu(L1)$_2$[(μ-CN)Au(CN)](H$_2$O)}[Au(CN)$_2$]	Yes	1D supramolecular chain	Distorted octahedron
(**3**) K{[Cu(L2)$_2$]$_2$[(μ-CN)$_2$Au]}[Au(CN)$_2$]$_2$Cl$_2$	Yes	1D supramolecular chain	Trigonal bipyramid
(**4**) {Cu(L3)$_2$[(μ-CN)AuCN]$_2$}·DMSO	No	Molecular entity	Distorted octahedron
(**5**) {Cu(L4)[(μ-CN)Au(CN)]}$_\infty$·CH$_3$CN	Yes	Coordination polymer	Tetrahedron

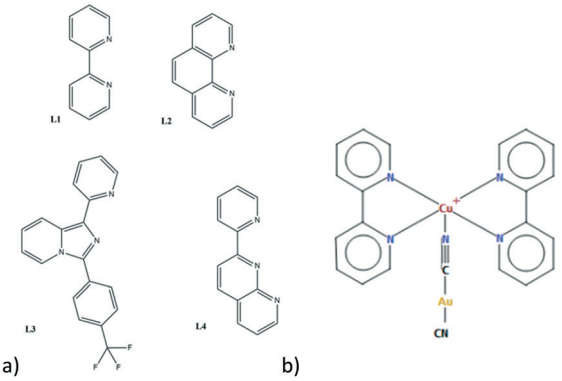

Fig. 2 (a) Scheme of employed organic ligands and (b) example of the structural formula of **1**–**6** complexes.

mixture was prepared using 100 mg of $K[Au(CN)_2]$ (molar ratio 1 : 2 : 2). The solutions were brought to boil with vigorous stirring and mixed. At the establishment of equilibrium (5 minutes) a green precipitate immediately appeared, which was redissolved after 30 minutes of stirring, forming a transparent light blue solution. After slow cooling to room temperature, the compound began to crystallize into dark navy-blue prisms. The crystals were separated by filtration, washed with cold water and dried. They are stable to air and humidity (yield: 96.8%, elemental analysis (%): calcd for $C_{24}H_{16}Au_2N_8Cu$: C, 32.35%; H, 2.51%; N, 12.83%; found: C, 32.65%; H, 2.41%; N, 12.86%. IR (ATR) cm^{-1}: 3394(s), 3208(s), 2926(s), 2856(s), 2145(s), 1605(s), 1572(m), 1467(m), 1429(m), 1301(m), 1243(m), 1019(m), 766(m), 733(m), 647(w)).

(2) {Cu(L1)$_2$[(μ-CN)Au(CN)](H$_2$O)}[Au(CN)$_2$]. 21.6 mg of $Cu(SO_4)\cdot 5H_2O$ and 27.0 mg of L1 were dissolved in 3 ml of deuterated water, and a second solution in the same solvent was prepared with 50.0 mg of $K[Au(CN)_2]$ (overall molar ratio 1 : 2 : 2) at the boiling point with vigorous stirring. The solutions were brought to boil with vigorous stirring and slowly mixed. At the establishment of equilibrium (5 min) a transparent pale green solution was finally obtained. After slow cooling and complete evaporation, transparent pale blue platelets were obtained, and crystals of compound **1** were found as impurity. Pure samples of **2** were obtained by dissolving **1** in aqueous ammonia. The crystals of **2** are stable to air and humidity. The suitable crystal of **2** for the SCXRD measurement was selected from the crystal mixture by colour observation under a microscope (yield: 97.5%, elemental analysis (%): calcd for $C_{24}H_{18}Au_2N_8OCu$: C, 32.31%; H, 2.03%; N, 12.56%; found: C, 32.55%; H, 2.10%; N, 12.72%. IR (ATR) cm^{-1}: 3389(s), 2171(m), 2148(s), 1607(m), 1569(w), 1476(m), 1446(s), 1156(m), 1102(w), 766(s), 731(m)).

(3) K{[Cu(L2)$_2$]$_2$[(μ-CN)$_2$Au]}[Au(CN)$_2$]$_2$Cl$_2$. 29.6 mg of $CuCl_2\cdot 2H_2O$ and 62.6 mg of L3 were dissolved in 10 ml of 50 : 50 EtOH/H_2O, and a different solution was prepared by dissolving 100 mg of $K[Au(CN)_2]$ (overall molar ratio 1 : 2 : 2) in 10 ml of 50 : 50 EtOH/H_2O. The solutions were brought to boil with vigorous stirring and then slowly mixed. At the establishment of equilibrium (5 min) a light green powder precipitated. Big dark green prismatic crystals were obtained from a solution in dimethyl sulfoxide of the previous powder kept at 277 K. Crystals have been separated by filtration, washed with cold water and dried. They are stable to air and humidity (yield: 94.5%, elemental analysis (%): calcd for $K_{1.5}Cl_{2.5}C_{54}H_{32}Au_3N_8OCu_2$: C, 37.21%; H, 1.85%; N, 10.22%; found: C, 37.33%; H, 1.89%; N, 10.35%. IR (ATR) cm^{-1}: 3567(m), 3486(m), 2198(s), 2140(s), 1522(m), 1434(s), 1148(m), 1109(m), 851(s), 720(s), 619(w)).

(4) {Cu(L3)$_2$[(μ-CN)AuCN]$_2$}·DMSO. 13.0 mg of $Cu(NO_3)_2\cdot 2.5H_2O$ and 35.0 mg of L3 were dissolved in 10 ml of a 50 : 50 EtOH/H_2O solution, and a separate solution in the same solvent mixture was prepared using 100 mg of $K[Au(CN)_2]$ (overall molar ratio 1 : 2 : 2). The solutions were brought to boil with vigorous stirring and slowly mixed. At the establishment of equilibrium (5 min) a pale olive-green powder precipitated. Red prismatic crystals were obtained by slow evaporation of a DMSO solution of the product. Crystals were separated by filtration, washed with cold water and dried. They are stable to air and humidity (yield: 96.5%, elemental analysis (%): calcd for $C_{44}H_{26}Au_2N_{10}SOCuF_3$: C, 40.14%; H, 2.14%; N, 10.64%; found: C, 40.23%; H, 2.11%; N, 10.96%. IR(ATR) cm^{-1}: 3440(m), 3085(w), 2188(m), 2140(s), 1607(m), 1518(m), 1322(s), 1171(m), 1129(s), 1067(s), 851(m), 785(m), 700(w)).

(5) {Cu(L4)[(μ-CN)Au(CN)]}$_\infty$·CH$_3$CN. 64.7 mg of $[Cu(NCCH_3)_4](PF_6)$ and 36.0 mg of L4 (molar ratio 1 : 1 : 1) were dissolved in 5 ml of acetonitrile, and a separate solution in the same solvent was prepared using 50.0 mg of $K[Au(CN)_2]$. The solutions were brought to boil with vigorous stirring and slowly mixed. At the establishment of equilibrium (5 min) a transparent dark red solution was obtained. After slow cooling to room temperature, the compound started to crystallise in transparent red prisms. The crystals were separated by filtration, washed with cold water and dried. They are stable to air and humidity. The employed synthetic procedure is similar to the one used by Leznoff and coworkers[38,48,49] and could be used with other ligands (yield: 90.5%, elemental analysis (%): calcd for $C_{32}H_{21}Au_2N_{11}Cu_2$: C, 35.56%; H, 1.95%; N, 14.25%; found: C, 35.35%; H, 1.89%; N, 14.33%. IR (ATR) cm^{-1}: 3073(w), 3002(w), 2152(s), 1604(m), 1515(w), 1449(w), 1254 (vs), 1170(s), 1037(s), 785(s), 771(m), 639(s), 519(w)).

(6) {Cu(L1)$_2$}[Au(CN)$_2$]$_2$·2Hg(CN)$_2$. Cocrystals of compound **1** with mercury cyanide were obtained by dissolving a small amount of **1** in dimethylformamide (DMF) with a strong excess of $Hg(CN)_2$. By slow evaporation, dark green platelets began to grow on the surface of the concomitantly crystallised mercury cyanide colourless prisms. The products are stable to air and humidity. The crystals have been isolated from the mercury cyanide crystals by washing with cold water or by mechanical separation (IR (ATR) cm^{-1} for **6**: 3384(s), 3197(s), 2922(s), 2856(m), 2139(s), 1606(s), 1568(m), 1475(m), 1431(s), 1320(m), 1148(m), 1011(m), 703(m), 626(m)).

X-ray crystallography

Single-crystal data were collected with a Gemini R Ultra diffractometer with graphite-monochromatized Mo-Kα radiation (λ = 0.71073 Å) for **1–6** using the ω-scan method. Data collection, data reduction and multi-scan absorption collection were performed in the CrysAlisPro software [CrysAlis PRO 1.171.38.46 (Rigaku OD, 2015)]. Using the Olex^2 program,[50] all structures were solved with direct methods with the SHELXS-14 solution program[51] and refined with full-matrix least-squares techniques on F^2 with the SHELXL-14 (ref. 52) refinement program. All non-hydrogen atoms were refined anisotropically. Hydrogen atom positions were calculated and refined riding on the corresponding bonded atoms. The graphics of the crystal structures were generated using Mercury 3.9.[53] CCDC codes 2078268 (**1**), 2078274 (**2**), 2078273 (**3**), 2078276 (**4**), 2078280 (**5**), and 2078267 (**6**) contain the supplementary crystallographic data for **1** to **6**.

For variable temperature measurements of compounds **1** and **6**, the crystals were cooled through a nitrogen flux from room temperature to 110 K for **1** and 150 K for **6**, with steps of 30 K h^{-1}. At each step, complete data collection was performed, keeping the temperature fixed, and the structures were solved and refined with the same programs and methods of environmental temperature measurements. CCDC codes 2078281–2078285 contain the supplementary crystallographic data for **1** and **6** at the measured temperatures.

For X-ray diffraction measurements under high-pressure conditions of compound **1**, two crystals were selected and loaded in an ETH-type diamond anvil cell (DAC).[54] A foil of T301 steel of 250 μm in thickness was used as a gasket to hold the crystals; the gasket was pre-indented to a thickness of approximately 100 μm before drilling a hole by spark-erosion (Ø 250 μm). The cell was loaded with an oil equivalent to that previously used in the literature[55] as a pressure-transmitting medium. The two different crystals were used to accurately centre the main diffraction peak positions to calculate the unit cell parameters and measure the diffraction intensities to refine the structural details and changes in HP. In the first case, we used a Siemens-Bruker P4 diffractometer (graphite monochromatized Mo-Kα radiation) equipped with a point detector. Along with the crystal (0.07 × 0.06 × 0.05 mm^3), a single crystal of quartz was loaded into the DAC, which allows the estimation of the internal pressure (P) on the base of its unit cell volume.[56] The uncertainty on P was estimated on the base of the standard deviation of the volume of the quartz unit cell. Data collection to determine the HP structure was performed on the same Gemini R Ultra diffractometer used for the ambient condition measurement; in the DAC was loaded the crystal (0.15 × 0.14 × 0.11 mm^3) together with three spherical rubies (Ø 10 μm), and the internal pressure was checked with a LABRAM HRVIS (Horiba–Jobin micro-Raman spectrometer) by measuring the shift of the ruby fluorescence line.[57] The single crystal X-ray data were collected at each pressure in four ω- and twelve φ-scans, covering the whole accessible reciprocal space (1785 frames, width 0.2°, exposure time = 60 s per frame, detector–sample distance 80 mm). The 171.35.21 version of CrysAlysPro (Rigaku Technologies) software has been used for data collection and reduction. Prior to integration, the diamond reflections were rejected. All high pressure structures have been refined with the same programs and methods of room temperature measurements. CCDC codes 2078286–2078289 contain the supplementary crystallographic data for **1** at the measured pressures. Details about the crystal structures are reported in the ESI.†

Vibrational spectroscopy

Infrared-attenuated total reflection (IR-ATR) spectra were collected using a Bruker Vertex 70 spectrometer equipped with a Harrick MVP2 ATR cell and using KBr optics and a DLaTGS detector. The spectra were acquired at 4 cm^{-1} resolution over 32 scans. FT-Raman spectra were obtained with a Bruker Vertex 70 spectrometer, equipped with a RAMII accessory, by exciting with a 1064 nm laser with a resolution of 4 cm^{-1}. Raman spectra of multiphase crystalline samples were obtained with a Horiba Jobin Yvon HR800 instrument equipped with an Olympus BX41 microscope. The samples were excited with 633 nm laser radiation with a magnification ratio of 50×. The results obtained for **3** in the presence of NH_3 will be discussed in the experimental results paragraph. In Table S1,† the diagnostic ν(CN) stretching frequencies of **1–6** are reported at atmospheric pressure.

Raman spectroscopy at high pressure

Raman spectra were acquired using a T64000 spectrometer from Horiba–Jobin–Yvon with an objective lens from Olympus (20×, focal distance f = 20.5 mm, numerical aperture NA = 0.35) coupled to a liquid nitrogen cooling CCD. To obtain high pressure conditions, a membrane diamond anvil cell was used with stainless steel gaskets with holes of ~150 μm as the chamber, indented to 80 μm. The chosen pressure transmitting medium was Nujol oil. In the same chamber, a small ruby chip was loaded to calibrate the pressure through the standard R1/R2 luminescence lines. To excite the sample, an argon laser emitting at 514.5 nm wavelength was used.

Vapochromism detection

Vapochromism has been detected by employing the apparatus reported in the ESI† (Fig. S16): test tubes containing crystals of complexes **1–5** have been sealed in a container under a vapour atmosphere. NH_3, pyridine, water, ethanol, methanol, tetrahydrofuran, dioxane, dichloromethane, chloroform, and *N*,*N*′-dimethylformamide have been checked. For each complex, changes have been observed within a week by means of UV-vis and vibrational spectroscopy. The UV-vis measurements have been performed on the powder sample with a Perkin Elmer Lambda 900 spectrophotometer in reflectance mode.

Results

Solid state characterisation of 1–6 under environmental conditions

The reaction of ligand L1 with Cu- and Au-salts gives rise to two crystalline products: (i) dark navy-blue crystals of $\{Cu(L1)_2[(\mu\text{-}CN)Au(CN)]\}[Au(CN)_2]$ (**1**) were obtained from ethanol, water or DMSO solutions, and (ii) pale blue crystals of $\{Cu(L1)_2[(\mu\text{-}CN)Au(CN)](H_2O)\}[Au(CN)_2]$ (**2**) were obtained from deuterated water or ammonia solutions. Compound **1** is characterised by $\{Cu(L1)_2[(\mu\text{-}CN)Au(CN)]\}^+$ cationic units involved in aurophilic chains and free dicyanoaurate anionic units (Fig. 3.1). These chains run along the *a* axis and are not homogeneous: strongly bonded trimeric units, formed from two cationic fragments and an anion with a + − + order, are connected by long Au⋯Au interactions (inner Au(1)⋯Au(2) distance = 3.293(1) Å, outer Au(1)⋯Au(1) distance = 3.653(1) Å, see Fig. 3.1). This last Au⋯Au interaction is quite long and can be due to the charge or steric repulsion between the bulkier fragments $\{Cu(L1)_2[(\mu\text{-}CN)Au(CN)]\}^+$, although the steric repulsion is minimised by the inversion of the copper position in relation to the gold chain. Cu(II) ions are surrounded by two L1 chelating ligands and an N-bonded cyanide, forming a distorted trigonal bipyramid of nitrogen donors. The Cu–dicyanoaurate fragment is quite linear ($\angle$(Au(1)–N1–Cu(1)) = 164.02(10)°). A third non-equivalent dicyanoaurate is inserted between the chains in a cradle formed by pyridyl rings (d(Au(3)⋯Cu(1)) = 4.294(4) Å, d(Au(3)⋯C(15)) = 3.318(5) Å and $\angle$(Au(1)–Cu(1)–Au(3)) = 148.17(10)°) and is not involved in strong directional interactions.

The crystal structure of **2** is analogous to that of $\{Zn(L1)_2[(\mu\text{-}CN)Au(CN)](H_2O)\}[Au(CN)_2]$.[29] This phase can be obtained in deuterated water, which stabilises this crystal phase through stronger internal hydrogen bonds due to deuterium substitution.[58] The same result can be obtained by recrystallisation of **1** from ammonia solutions where a slow loss of the monodentate ligand occurs. It is interesting to consider that the Zn(II)–L1–dicyanoaurate system forms

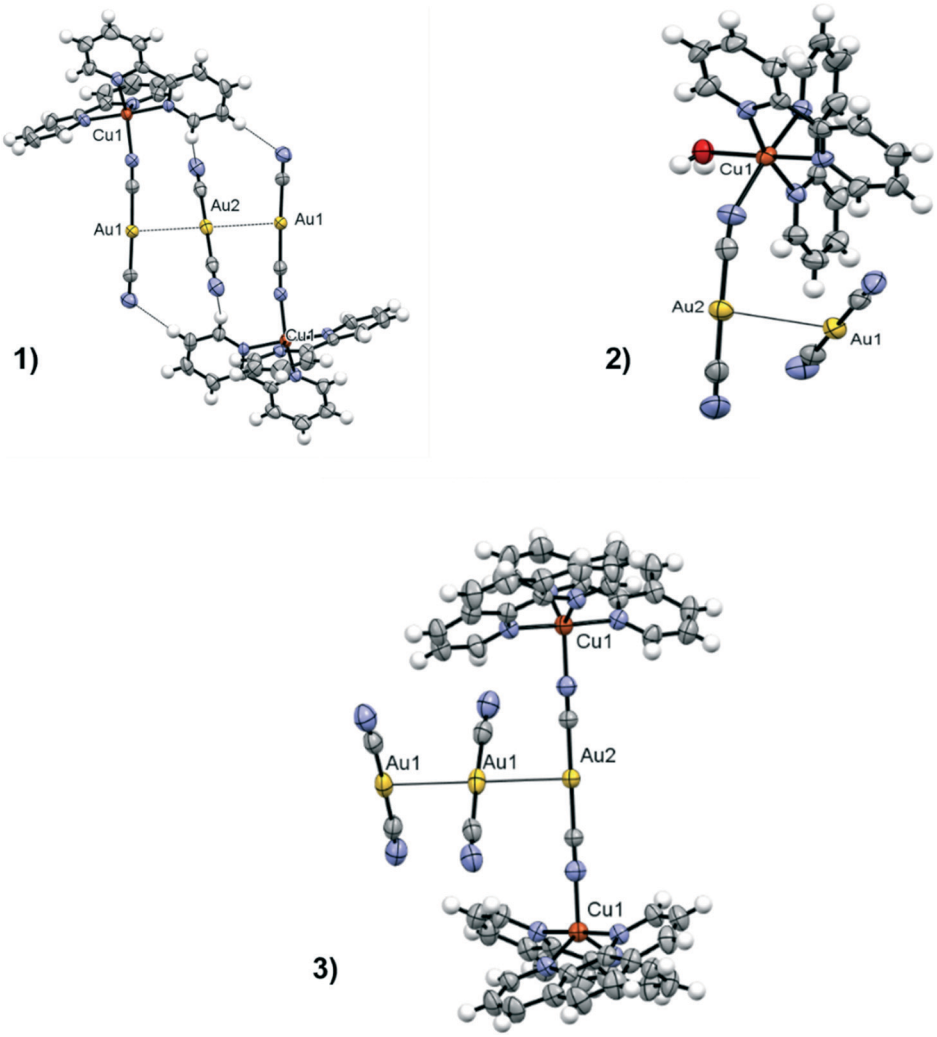

Fig. 3 ORTEP plots of the trimeric aurophilic bonded structure of compound **1**, of the aurophilic-hydrogen bonded aggregate in compound **2** and of the aurophilic chains of compound **3** (50% probability) (color code: white, hydrogen; gray, carbon; blue, nitrogen; yellow, gold; orange, copper; red, oxygen).

the hydrated complex both in solution and in the solid state (but not in the gas phase), while for Cu(II) the situation is opposite. In almost all solvents the anhydrous **1** complex is formed, probably for a softer character of the metal centre, while the formation of hydrated complex **2** must be promoted with some expedients (stronger hydrogen bond of deuterated water or sacrificing one ammonia ligand).

In the crystal structure of **2**, a cationic molecular complex $\{Cu(L1)_2[(\mu\text{-}CN)Au(CN)](H_2O)\}^+$ and an anionic $[Au(CN)_2]^-$-complex are present, linked by aurophilic interactions and hydrogen bonds (Fig. 3.2). A 2D supramolecular network similar to the network $\{M(L)_2[(\mu\text{-}CN)M'(CN)](H_2O)\}[M'(CN)_2]$ (M = Zn, Mn, Ni, Cd; L = 1,10-phenanthroline, 2,2′-bipyridine; M′ = Ag, Au) was observed (see Fig. 3.2).[29,59–62] The general structural characteristics observed for $\{Zn(L1)_2[(\mu\text{-}CN)Au(CN)](H_2O)\}[Au(CN)_2]$ are maintained, but the two compounds are not perfectly isomorphic, although they crystallise in the same space group type $P2_1/c$. Moving from the zinc to the copper complex, the a and c axes contract by 0.107 Å and 0.03 Å, respectively, while the b axis expands by 0.101 Å and the β angle increases by 0.9°. These metric differences can probably explain the impossibility of obtaining solid solutions between these compounds. In fact, when compound **2** and the zinc analogue are dissolved in DMF or ethanol, crystals of both the complexes are obtained separately. These characteristics can be explained by the elongated octahedral environment of the Cu(II) ion due to the pseudo Jahn–Teller effect (d(Cu(1)–N(6)) = 2.022(5) Å with respect to d(Cu(1)–N(7)) = 2.291(4) Å). This distortion is propagated within the structure through the dicyanoaurate fragment that is more parallel to the copper-cyanide axes with respect to the zinc analogue [$\angle$(Cu(1)–N(1)–N(2)) = 151.55(8)° and $\angle$(Zn(1)–N(3)–N(4)) = 155.42(10)°]. This arrangement decreases from 3.2673(6) Å to 3.2360(5) Å for the Au(1)···Au(2) distance and from 2.802(5) Å and 2.769(5) Å to 2.760(4) Å and 2.726(4) Å for the two hydrogen bonds connecting the water ligand and the terminal cyanides (calculated on the oxygen–nitrogen donor acceptor distance). Thus, the supramolecular network in the Cu complex is more compact than that in the Zn derivative.[63] Besides, in all the octahedral complexes reported in this work, the L ligands are in a *cis* configuration, unlike the case of the ethylenediamine (or similar substituted ligands) derivatives $[M(en)_2[M'(CN)_2]_2\}$ (M = Zn, Cu, M′ = Ag, Au), which are invariantly in a *trans* configuration.[64–71] This difference can be attributed to steric factors.

By employing L2, green crystals of $K\{[Cu(L2)_2]_2[(\mu\text{-}CN)_2Au]\}[Au(CN)_2]_2Cl_2$ (**3**) were obtained from DMSO solution. In this case, the Cu(II) centre is penta-coordinated with two chelating ligands and a dicyanoaurate, forming a nearly perfect trigonal bipyramid. Two copper centres are bonded to the same dicyanoaurate, forming a positively charged $\{[Cu(L2)_2]_2[(\mu\text{-}CN)_2Au]\}^{3+}$ fragment (see Fig. 3.3). This fragment interacts with two other dicyanoaurates through short aurophilic interactions [d(Au(1)···Au(2)) = 3.216(2) Å, d(Au(1)···Au(1)) = 3.171(2) Å] forming Au chains along the a axis. In these chains there are one positive fragment and two negative fragments, with an anti-coulombic 2+ − − 2+ order. The two free dicyanoaurates are rotated with respect to each other and with respect to the positively charged fragment [torsional angle (N(2)–Au(2)–Au(1)–N(1)) = 39.93(8)° and torsional angle (N(1)–Au(1)–Au(1)–N(1)) = 79.95(8)°, see Fig. 3.3]. The aromatic rings of L2 bonded to the Cu(II) centres form cradles, which define channels filled with a residual disordered electron density. This electron density was interpreted as disordered potassium and chloride ions.

With strongly substituted L3, we obtained $\{Cu(L3)_2[(\mu\text{-}CN)AuCN]_2\}\cdot$DMSO (**4**) (Fig. 4.4). Both dicyanoaurate anions are directly coordinated to the copper centre, forming a distorted octahedral environment with the aromatic ligands. The pseudo Jahn–Teller effect is quite strong, shortening the axial distance Cu(1)–N(3) (2.012(5) Å) compared to the equatorial Cu(1)–N(4) and Cu(1)–N(1) (2.238(4) Å and 2.158(5) Å, respectively). Also in this case, there is a strong similarity with the zinc complex $\{Zn(L3)_2[(\mu\text{-}CN)Au(CN)]_2\}\cdot$DMSO,[29] not considering the inherent distortion. However, with copper it was not possible to obtain the homologous coordination polymer from DMF.[29] Imidazo[1,5*a*]pyridines may form mono- and bis-coordinated complexes with copper,[45,72–74] but in this case no mono-chelated crystalline product was detected. In the CSD the majority of the complexes present Cu(I) as the metal centre (17 of 28 crystal structures reported). Complex **4** has the peculiarity of being one of the stable imidazo[1,5*a*]pyridine complexes formed by the Cu(II) ion.[75–81] The stability of Cu(II) may be related to the presence of dicyanoaurate in the first coordination sphere. Compound $Cu(L4)[(\mu\text{-}CN)Au(CN)]\}_\infty\cdot CH_3CN$ **5** has Cu(I) cations with a tetrahedral environment of L4.[82] It forms a wavy 1D coordination polymer with bridged dicyanoaurate. The ribbons are arranged in parallel and interact in couples through strong aurophilic interactions (d(Au(1)···Au(2)) = 3.134(1) Å, see Fig. 4.5). Some other Cu(I)–dicyanoaurate compounds have been reported, but no nitrogen chelating ligand has been used until now.[38,48,49] In this system binuclear Cu(I) products have been reported using CuCN with the same ligand,[2,8,43] but no similar products have been obtained in this case.

Vapochromism solid state characterisation

Heterobimetallic coordination polymers based on the dicyanoaurate unit have shown to be remarkable for sensing application.[17,18,37] The mechanisms have been studied and can be explained either by selective complexation of the host's vapour molecules with the metal (for example in $Cu[Au(CN)_2]_2$)[17] or by some weak interaction that changes the electronic properties of the compound.[83] We verified the response of our compounds to several different volatile molecules and the most interesting behaviour has been found with crystals of **3** in the presence of ammonia vapour. The green crystals change their electronic properties and turn blue, but completely lose their crystalline structure, according to the PXRD measurement. This modification is completely reversible, either by exposure to heat (330 K for 15 minutes)

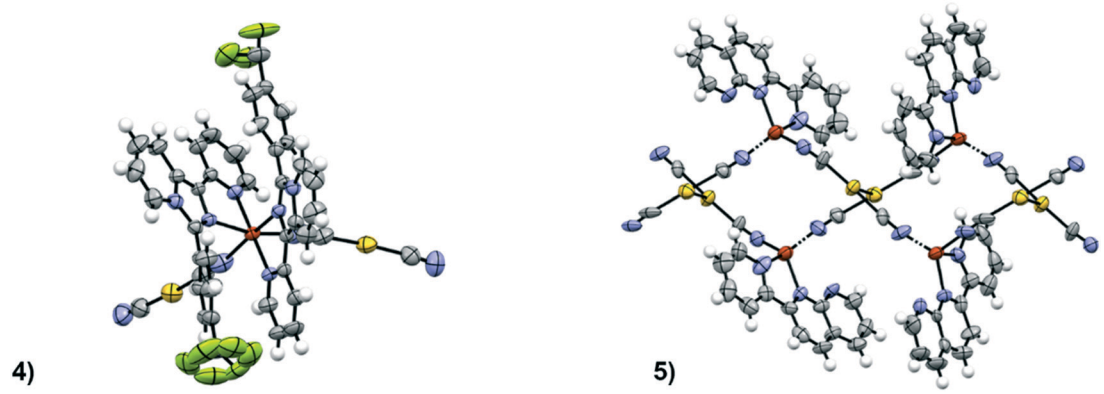

Fig. 4 ORTEP plots of the molecular structure of compound **4** and of the polymeric structure of compound **5** (50% probability) (color code: white, hydrogen; gray, carbon; blue, nitrogen; yellow, gold; orange, copper; red, oxygen; light green, fluorine).

or by redissolving and recrystallizing the compound in DMSO or THF. The compound is stable for several cycles, although the mono-crystallinity is lost after the first ammonia passage. The interaction with ammonia was studied with UV-vis and micro-IR spectroscopy. In the UV-visible spectra of **3** there is a clear shift in the π–π* inter-ligand ultraviolet band of L3 from 351 nm to 299 nm, while the visible region is less indicative because it is too broad (Fig. 5b). More detailed information has been obtained from vibrational data. The IR spectrum of the blue product presents new signals related to the presence of ammonia at 3300, 1630, 1275 and 760 cm^{-1} (Fig. 5a). These bands are attributable to the stretching, deformation and rocking modes of NH_3 molecules in copper complexes.[84,85] It has been suggested that hydrogen bonding shifts signals at higher frequencies, and the most sensitive shift is generally observed for the rocking mode,[86] as observed in our product. The presence of hydrogen bonds is confirmed by the broadening of stretching mode signals. Some water molecules may also be present and involved in hydrogen bonding, but no sure assignment can be done due to the proximity of the signals.[87] In the spectrum of the blue product, there are some bands attributable to the free L2 and we observed a different multiplicity of cyanide signals. These features suggest that L2 is partially substituted by ammonia in the first coordination sphere of Cu(II), causing a large modification in the crystal environment.[88]

It can be supposed that the ammonia molecules penetrate the crystal architecture through the disordered channels between the L2 ligands, but further studies should be carried out. Furthermore, the spectrum of the product after heating (pink line in Fig. 5a) is analogous to that of **3**, suggesting that ammonia absorption is completely reversible.

Environmental condition solid state characterisation of co-crystals with $Hg(CN)_2$

Starting from the assumption that $\{Cu(L)_2[Au(CN)_2]\}^+$, as we demonstrated earlier,[29] is quite stable in solution, we tried to form co-crystals by dissolving the previously described solids with other d^{10} metal complexes, such as mercury halides and pseudohalides.

When **1** is dissolved in solution in the presence of a strong excess of $Hg(CN)_2$, dark green crystals of **6** are formed, which show a peculiar architecture. In this compound, the dicyanoaurate is detached from the copper centre, leaving a distorted tetrahedral $[Cu(L)_2]^{2+}$ molecule ($\angle$(N(5)–Cu(1)–N(5)) = 104.3(1)° for **6**), and forms aurophilic attracted anion pairs with a tilted conformation (d(Au(1)···Au(1)) = 3.232(3) Å and $\angle$(C(1)–Au(1)···Au(1)–C(1)) = 59.90(10)° for **6**, see Fig. 6.6b). These pairs of dicyanoaurates interact with the mercury(II) cyanide molecules through a long secondary interaction (d(N(1)···Hg(1)) = 2.860(5) Å for **6**). This is not the only case

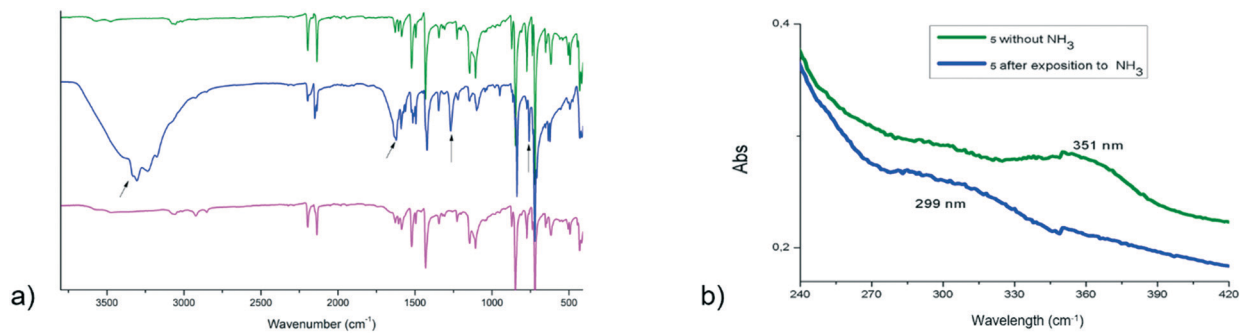

Fig. 5 (a) Infrared spectra and (b) UV-vis absorption spectra of (**3**) (in green) and of the products obtained after ammonia exposure (in blue) and after ammonia removal (in pink).

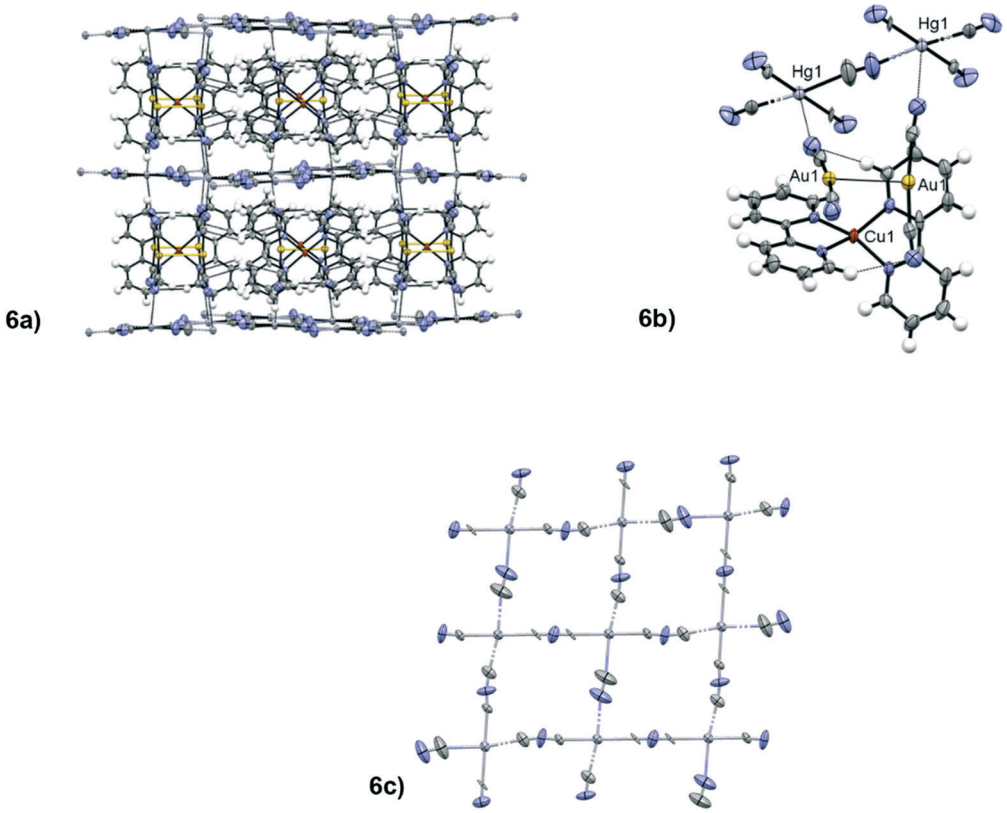

Fig. 6 ORTEP plots of the polymeric structure of the supramolecular structure of compound **6** (6a), a fragment of the complex architecture (6b) and a detail on the $HgCN_2$ disordered layer (6c) (50% probability) (colour code: white, hydrogen; gray, carbon; blue, nitrogen; yellow, gold; orange, copper; red, oxygen; light gray, mercury; light green, fluorine; green, chlorine).

of Hg···NC contacts: $Hg(CN)_2$ and its adducts present similar interactions.[89–91] In the crystal structure of **6** the disordered mercury cyanide molecules form layers that separate the ordered molecular part of the crystal packing (see Fig. 6.6a). The disorder of the mercury cyanides in these layers can be described with a network of randomly parallel and perpendicular molecules of $Hg(CN)_2$, which can interact with each other with long CN···Hg contacts (around 3 Å, see Fig. 6.6c). Any attempt to find an ordered supercell at room temperature failed due to the absence of any weak superlattice diffraction reflections. In the next sections, the attempt to force a low temperature ordering will be discussed. The trimetallic architecture observed in **6** is an example in which the cocrystal does not maintain the original unit, so the dicyanoaurate anion interacts separately from the other d^{10} metal centre. The results obtained with **6** open the way for further studies toward other molecular fragments involving metal centres that can interact more strongly with Au(I), obtaining multi-metallic aurophilic supramolecular architectures.

High-pressure solid-state characterization of 1

High pressure measurements on gold complexes showing aurophilic interactions have been performed in the past, especially to modulate the luminescence emission or to study polymorphism.[92–97] Further investigations have been done on inorganic salts like AuX or $M[Au(CN)_2]_n$ to study the solid state compressibility of peculiar arrangements of gold atoms.[98–101] By selecting **1** as a prototype of the supramolecular architectures formed from the dicyanoaurate and metal-gold complexes with a chelating ligand, high pressure and low temperature measurements have been performed. To our knowledge, no HP-VT study has been performed so far on this type of bimetallic supramolecular material, other than on coordination polymers based on iron–dicyanoargentate or dicyanoaurate for spin transition studies.[102,103]

Raman spectra at variable pressures have been recorded in the 50–1300 cm^{-1} range. The assignment of vibrational modes has been done by comparison with vibrational spectra of 2,2′-bipyridine,[104] L1–Cu(II) complexes[105] and $K[Au(CN)_2]$[106] and is reported in Table S21.†

In the 1300–600 cm^{-1} region there is mainly C–C and C–N ring stretching, along with in-plane C–H and C–C–C bending. The pressure effect on these modes, in the interval explored, is mainly a moderate blue shift. By considering a linear volume reduction as a consequence of the applied pressure, from ambient pressure to 1.59 GPa the cell volume undergoes a 23% contraction, and this probably does not significantly affect the geometry of coordinated L1. A similar behaviour is detected for the ring bending mode at 371 cm^{-1}, which blue shifts to 383 cm^{-1} at 1.59 GPa. The vibrational stretching

involving Cu(II) can be attributed to the 268 cm^{-1} band ($\nu_{Cu-N(L1)}$) that in addition to a broadening is not significantly affected by the pressure variation. The modes attributable to the $[Au(CN)_2]^-$ fragment show an interesting behaviour: from ambient pressure to 0.8 GPa they undergo a decrease in intensity and from 1.1 GPa they are no longer detectable from the background (see the rectangle in the spectrum at 0.8 GPa in Fig. 7a). We may attribute the bands centred at 248 cm^{-1} to the Au–CN bending, the strong band at 408 cm^{-1} to the Cu–N(C) stretching and the weak band at 470 cm^{-1} to the $\nu_{Au-C(N)}$ stretching. Starting from 1.1 GPa, two bands appeared at 401 and 419 cm^{-1}, and this suggests a phase change in the crystal structure, mainly affecting the $[Au(CN)_2]^-$ units. Consequently, high pressure Raman measurements show modifications in the 0.8–1.2 GPa range and in the 1.4–1.7 GPa range (see Fig. 7a and b), suggesting two main events in a pressure range below 3.6 GPa. In particular, Raman peaks increase their linewidths above 1.4

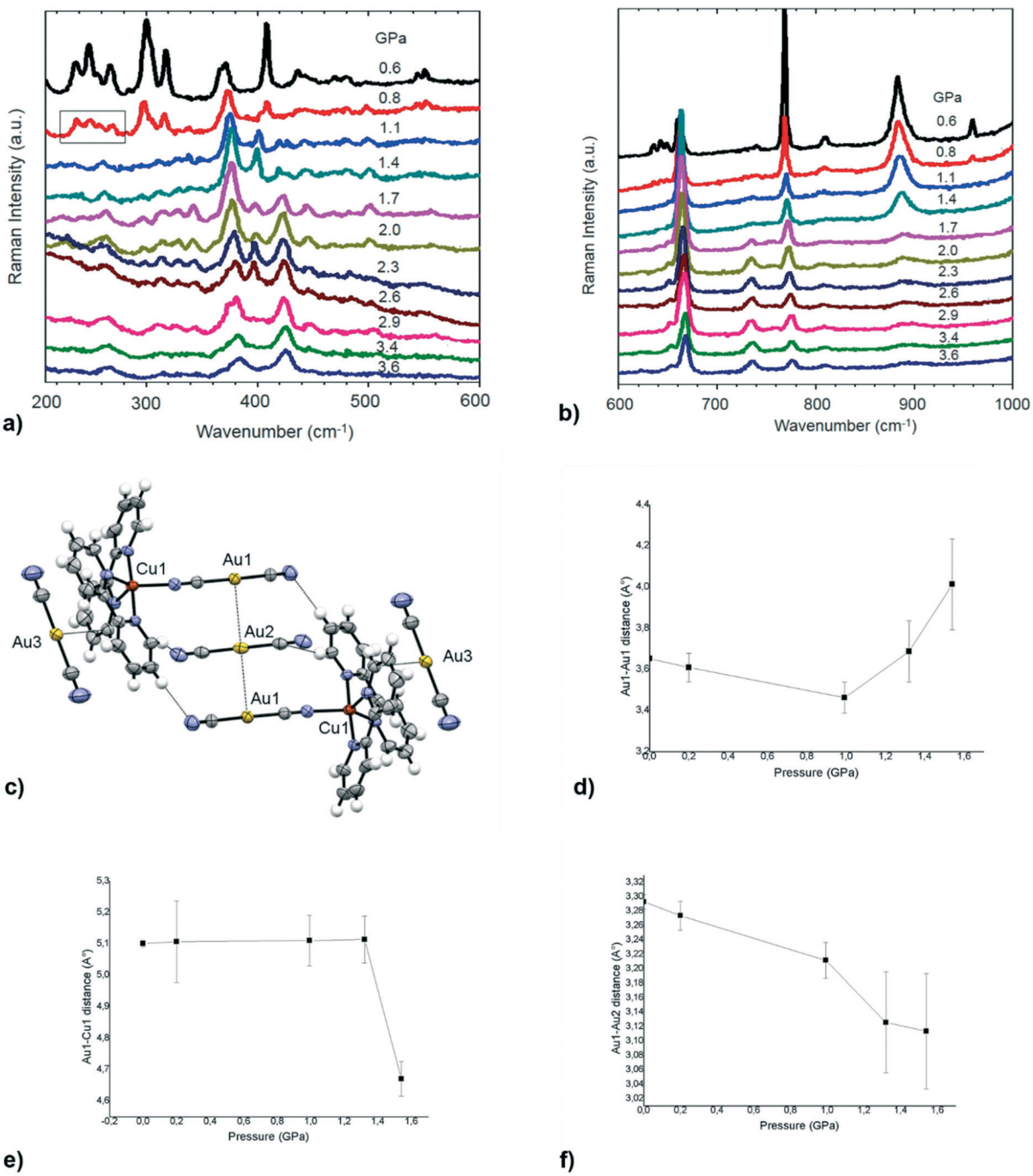

Fig. 7 High pressure Raman spectra in the 200–600 cm^{-1} (a) and 600–1000 cm^{-1} (b) spectral ranges of **1** from 0.6 to 3.6 GPa. (d), (e) and (f) are the evolution of heavy atom distances within the crystal structure of **1** (c) between 0 and 1.5 GPa.

GPa, suggesting an increase in the disorder or even the onset of amorphization. The presence of a series of modifications at relatively low pressure is typical for soft molecular materials.[107,108] Inspired by these results, we performed SC-XRD studies on **1** at high pressure. However, structural studies of single crystals could be possible up to 1.5 GPa for sample amorphization. At the same time, the low symmetry and the complexity of the crystal structure of **1** made it impossible to have a good parameter/data ratio. For this reason, in the following discussion only cell parameters and heavy atoms (the most important scatterer) will be presented.

When looking at the SC-XRD data, the *b* axis is the most influenced by pressure, decreasing by more than 0.9 Å (Fig. S11b†), compared to a lengthening of 0.1 Å of the *c* axis (Fig. S11b†) and a decrease of 0.3 Å of the *a* axis (Fig. S11b†). This suggests greater compressibility in the direction parallel to the dicyanoaurates and greater rigidity due to steric hindrance in the other two perpendicular directions. In the pressure range of 0–1.5 GPa, some general variation in the distances between metal atoms can be observed. The geometry of the $\{Cu(L1)_1[Au(CN)_2]\}^+$ fragment, evaluated through the Cu(1)–Au(1) distance, remains unaltered up to 1.3 GPa. After this pressure, we observe a shortening of 0.4 Å of this distance (see Fig. 7f), suggesting a strong distortion, probably a closure of the Cu–CN–Au angle. In the same pressure range, the two aurophilic contacts have different behaviours. The shorter Au(1)···Au(2) distance has an intense compression of 0.27 Å (see Fig. 7e), while the longer Au(1)···Au(1) distance, after lighter compression before 1.0 GPa, exhibits a decisive lengthening (see Fig. 7d). This anomalous behaviour can also be probably attributed to the distortion of the cationic complex and to the shift of the molecular fragments in the direction of maximal compression. It is also interesting to note that the Au(3)···Cu(1) distance, involving the dicyanoaurate unit inserted in the cradle of the pyridine rings, has an intense shortening of 0.3 Å before 1.3 GPa and a lengthening after this pressure (see Fig. S19d† and 7c). This behaviour may suggest the presence of an attractive force between the pyridyl groups of L1 and the dicyanoaurate complex with a minimum in the energy surface at about 3.95 Å, the distance after which the interaction becomes repulsive. The existence of this attraction is also suggested by the high probability that the linear dicyanoaurate shows this arrangement in crystals presenting aromatic ligands.[109] All these data, with the analysis of the evolution of the cell parameters (see the ESI† for details), suggest the presence of a distortive isosymmetric phase transition between 1.3 and 1.5 GPa.

Variable temperature SC-XRD characterization of 1 and 6

Variable temperature studies on **1** and **6** have been performed for three reasons: 1) to study the possibility of a phase transition analogous to that found under high pressure conditions for **1**; 2) to study the temperature dependence of weak interaction distances and structural parameters; 3) to search for an ordered supercell for **6**. Analogous studies on dicyanoaurate salts, coordination polymers or gold complexes to study the thermal expansion and luminescence have been reported in the literature.[19,21,22,93,110–112]

1 and **6** have been studied with SC-XRD from 150 K to 343 K for **1** (200 K to 343 K for **6**). No distortive isosymmetric phase transition has been found, but a continuous temperature dependence of the cell parameters. Unlike pressure, temperature has a small effect on the reticular parameters and distances in **1**, probably due to the high steric hindrance of the molecular fragments. A specific graph for each main structural and cell parameter can be found in the ESI† (Fig. S14 and S15). A more visible effect can be observed on the motion component of the atoms, especially the oscillation of the C(3) N(3) cyanide of the free dicyanoaurate around the centre of Au(3) (see Fig. S16† for the main motion components of N3).

In **6**, although no ordered supercell has been found, more pronounced effects on the overall architecture have been observed between 200 K and 343 K. In this range, the Au(1)··· Au(1) aurophilic interaction has a lengthening of 0.04 Å (see Fig. S19a†) and the arrangement of the couple of dicyanoaurate has a slightly more tilted conformation (Fig. S19c†). The molecular fragment $[Cu(L1)_2]^{2+}$ becomes slightly more tetrahedral as the temperature rises (Fig. S19b†). This is probably due to the increase in the interplanar distance between mercury cyanide layers (from 11.019(7) Å at 200 K to 11.044(8) Å at 343 K) and the lengthening of the CN···Hg(1) distance of 0.04 Å that connects the layers (see Fig. S18d†).

Conclusions

In this article, we demonstrate the possibility of systematically obtaining a family of supramolecular architectures constructed by aurophilic interactions based on copper–dicyanoaurate molecular fragments in the presence of chelating ligands. These results have been possible due the tendency of Cu(II) to be coordinated by two chelating ligands, leaving one or two free sites to the attachment of dicyanoaurate. The stability of these bis-chelated Cu(II)–Au(I) fragments allows obtaining co-crystals with other d^{10} metals, even in the absence of aurophilic interactions, opening the way for aurophilic-based crystal engineering between bimetallic complexes. The new bimetallic materials were investigated for vapochromism, and one of them shows a reversible response to the presence of ammonia, measurable by UV-vis and IR vibrational spectroscopy. Finally, the first high pressure–variable temperature study on a bimetallic supramolecular aurophilic architecture was performed. A series of isosymmetric distortive phase transitions due to high pressure have been detected by Raman spectroscopy, but the effect of these two parameters on the crystal structure is, in general, not very strong, probably due to the high steric hindrance. In particular, aurophilic interactions are not necessarily involved in the main movements in the crystal structure, while some distortion around copper centres can be preferred. However, more studies must be done to unravel the possible transformations of these materials with high

pressure and variable temperature and, possibly, to systematically achieve abnormal phenomena such as giant negative linear compressibility.

Conflicts of interest

There are no conflicts to declare.

References

1 J. Gil-Rubio and J. Vicente, *Chem. – Eur. J.*, 2018, **24**, 32–46.
2 E. V. Alexandrov, A. V. Virovets, V. A. Blatov and E. V. Peresypkina, *Chem. Rev.*, 2015, **115**, 12286–12319.
3 M. J. Katz, K. Sakai and D. B. Leznoff, *Chem. Soc. Rev.*, 2008, **37**, 1884–1895.
4 A. Canumalla, C. F. Shaw and F. E. Wagner, *Inorg. Chem.*, 1999, **38**, 3268–3269.
5 R. D. Hancock, N. P. Finkelstein and A. Evers, *J. Inorg. Nucl. Chem.*, 1972, **34**, 3747–3751.
6 X.-B. Wang, Y.-L. Wang, J. Yang, X.-P. Xing, J. Li and L.-S. Wang, *J. Am. Chem. Soc.*, 2009, **131**, 16368–16370.
7 M. Bardají and A. Laguna, *J. Chem. Educ.*, 1999, **76**, 201.
8 H. Schmidbaur and A. Schier, *Chem. Soc. Rev.*, 2012, **41**, 370–412.
9 H. Schmidbaur and A. Schier, *Chem. Soc. Rev.*, 2008, **37**, 1931–1951.
10 H. Schmidbaur, *Gold Bull.*, 2000, **33**, 3–10.
11 J. A. Hill, A. L. Thompson and A. L. Goodwin, *J. Am. Chem. Soc.*, 2016, **138**, 5886–5896.
12 J. A. Hill, C. A. Murray, C. C. Tang, P. M. M. Thygesen, A. L. Thompson and A. L. Goodwin, *Chem. Commun.*, 2019, **55**, 5439–5442.
13 J. Suárez-Varela, H. Sakiyama, J. Cano and E. Colacio, *Dalton Trans.*, 2007, 249–256, DOI: 10.1039/B611684A.
14 A. B. Cairns, J. Catafesta, C. Levelut, J. Rouquette, A. van der Lee, L. Peters, A. L. Thompson, V. Dmitriev, J. Haines and A. L. Goodwin, *Nat. Mater.*, 2013, **12**, 212–216.
15 E. J. Fernandez, A. Laguna and J. M. Lopez-De-Luzuriaga, *Dalton Trans.*, 2007, 1969–1981, DOI: 10.1039/b702838p.
16 G. L. Cui, X. Y. Cao, W. H. Fang, M. Dolg and W. Thiel, *Angew. Chem., Int. Ed.*, 2013, **52**, 10281–10285.
17 J. Lefebvre, R. J. Batchelor and D. B. Leznoff, *J. Am. Chem. Soc.*, 2004, **126**, 16117–16125.
18 M. J. Katz, T. Ramnial, H.-Z. Yu and D. B. Leznoff, *J. Am. Chem. Soc.*, 2008, **130**, 10662–10673.
19 L. Wang, H. Luo, S. Deng, Y. Sun and C. Wang, *Inorg. Chem.*, 2017, **56**, 15101–15109.
20 X. Zhang, B. Li, Z.-H. Chen and Z.-N. Chen, *J. Mater. Chem.*, 2012, **22**, 11427–11441.
21 A. L. Goodwin, B. J. Kennedy and C. J. Kepert, *J. Am. Chem. Soc.*, 2009, **131**, 6334–6335.
22 J. L. Korčok, M. J. Katz and D. B. Leznoff, *J. Am. Chem. Soc.*, 2009, **131**, 4866–4871.
23 R. K. Arvapally, P. Sinha, S. R. Hettiarachchi, N. L. Coker, C. E. Bedel, H. H. Patterson, R. C. Elder, A. K. Wilson and M. A. Omary, *J. Phys. Chem. C*, 2007, **111**, 10689–10699.
24 X. He and V. W.-W. Yam, *Coord. Chem. Rev.*, 2011, **255**, 2111–2123.
25 J. R. Thompson, M. J. Katz, V. E. Williams and D. B. Leznoff, *Inorg. Chem.*, 2015, **54**, 6462–6471.
26 M. J. Katz and D. B. Leznoff, *J. Am. Chem. Soc.*, 2009, **131**, 18435–18444.
27 A. S. Abouelwafa, C. E. Anson, A. Hauser, H. H. Patterson, F. Baril-Robert, X. Li and A. K. Powell, *Inorg. Chem.*, 2012, **51**, 1294–1301.
28 T. P. Seifert, V. R. Naina, T. J. Feuerstein, N. D. Knöfel and P. W. Roesky, *Nanoscale*, 2020, **12**, 20065–20088.
29 E. Priola, G. Volpi, R. Rabezzana, E. Borfecchia, C. Garino, P. Benzi, A. Martini, L. Operti and E. Diana, *Inorg. Chem.*, 2020, **59**, 203–213.
30 W. A. E. McBryde, *A critical review of equilibrium data for proton- and metal complexes of 1,10-phenantroline, 2,2'-bipyridyl and related compounds*, IUPAC CHEMICAL DATA SERIES, Oxford, 1978.
31 K. Yamasaki and M. Yasuda, *J. Am. Chem. Soc.*, 1956, **78**, 1324–1324.
32 M. Yasuda, K. Sone and K. Yamasaki, *J. Phys. Chem.*, 1956, **60**, 1667–1668.
33 B. Murphy, M. Aljabri, A. M. Ahmed, G. Murphy, B. J. Hathaway, M. E. Light, T. Geilbrich and M. B. Hursthouse, *Dalton Trans.*, 2006, 357–367, DOI: 10.1039/B509070A.
34 B. Murphy and B. Hathaway, *Coord. Chem. Rev.*, 2003, **243**, 237–262.
35 B. J. Hathaway, *Coord. Chem. Rev.*, 1981, **35**, 211–252.
36 B. J. Hathaway, A new look at the stereochemistry and electronic properties of complexes of the copper(II) ion, in *Complex Chemistry, Structure and Bonding*, Springer, Berlin, Heidelberg, 1984, vol. 57.
37 J. Lefebvre, J. L. Korčok, M. J. Katz and D. B. Leznoff, *Sensors*, 2012, **12**(3), 3669–3692.
38 B. R. Varju, J. S. Ovens and D. B. Leznoff, *Chem. Commun.*, 2017, **53**, 6500–6503.
39 D. B. Leznoff, B.-Y. Xue, C. L. Stevens, A. Storr, R. C. Thompson and B. O. Patrick, *Polyhedron*, 2001, **20**, 1247–1254.
40 S. Kitagawa, M. Munakata and A. Higashie, *Inorg. Chim. Acta*, 1984, **84**, 79–84.
41 M. M. Turnbull, G. Pon and R. D. Willett, *Polyhedron*, 1991, **10**, 1835–1838.
42 F. Grifasi, E. Priola, M. R. Chierotti, E. Diana, C. Garino and R. Gobetto, *Eur. J. Inorg. Chem.*, 2016, **2016**, 2975–2983.
43 A. Giordana, E. Priola, G. Gariglio, E. Bonometti, L. Operti and E. Diana, *Polyhedron*, 2021, **198**, 115059.
44 G. Volpi, *J. Chem. Educ.*, 2016, **93**, 891–897.
45 G. Volpi, E. Priola, C. Garino, A. Daolio, R. Rabezzana, P. Benzi, A. Giordana, E. Diana and R. Gobetto, *Inorg. Chim. Acta*, 2020, **509**, 119662.
46 G. Volpi, G. Magnano, I. Benesperi, D. Saccone, E. Priola, V. Gianotti, M. Milanesio, E. Conterosito, C. Barolo and G. Viscardi, *Dyes Pigm.*, 2017, **137**, 152–164.
47 A. Giordana, E. Priola, E. Bonometti, P. Benzi, L. Operti and E. Diana, *Polyhedron*, 2017, **138**, 239–248.
48 J. S. Ovens, P. R. Christensen and D. B. Leznoff, *Chem. – Eur. J.*, 2016, **22**, 8234–8239.

49 J. S. Ovens and D. B. Leznoff, *ChemPlusChem*, 2016, **81**, 842–849.
50 O. V. Dolomanov, L. J. Bourhis, R. J. Gildea, J. A. K. Howard and H. Puschmann, *J. Appl. Crystallogr.*, 2009, **42**, 339–341.
51 G. M. Sheldrick, *Acta Crystallogr., Sect. A: Found. Crystallogr.*, 2008, **64**, 112–122.
52 G. M. Sheldrick, *Acta Crystallogr., Sect. A: Found. Adv.*, 2015, **71**, 3–8.
53 C. F. Macrae, P. R. Edgington, P. McCabe, E. Pidcock, G. P. Shields, R. Taylor, M. Towler and J. van De Streek, *J. Appl. Crystallogr.*, 2006, **39**, 453–457.
54 R. Miletich, D. R. Allan and W. F. Kuhs, *Rev. Mineral. Geochem.*, 2000, **41**(1), 445–519.
55 F. Bertolotti, N. Curetti, P. Benna and G. Gervasio, *J. Mol. Struct.*, 2013, **1041**, 106–112.
56 R. J. Angel, D. R. Allan, R. Miletich and L. W. Finger, *J. Appl. Crystallogr.*, 1997, **30**, 461–466.
57 H. K. Mao, J. Xu and P. M. Bell, *J. Geophys. Res.: Solid Earth*, 1986, **91**, 4673–4676.
58 S. Scheiner and M. Čuma, *J. Am. Chem. Soc.*, 1996, **118**, 1511–1521.
59 G. F. Xu, Z. Q. Liu, H. B. Zhou, Y. Guo and D. Z. Liao, *Aust. J. Chem.*, 2006, **59**, 640–646.
60 M. Monim-ul-Mehboob, M. Ramzan, T. Ruffer, H. Lang, S. Naddem, M. Akhtar and S. Ahmad, *Z. Naturforsch.*, 2013, **68**, 161–167.
61 Y. Guo, Y. Ma, N. Zhou, Z. Q. Liu, Q. L. Wang, S. P. Yan and D. Z. Liao, *Z. Anorg. Allg. Chem.*, 2010, **636**, 865–871.
62 J. Qu, W. Gu and X. Liu, *J. Coord. Chem.*, 2008, **61**, 618–626.
63 E. R. T. Tiekink, *Coord. Chem. Rev.*, 2014, **275**, 130–153.
64 P. M. Aguiar, M. J. Katz, D. B. Leznoff and S. Kroeker, *Phys. Chem. Chem. Phys.*, 2009, **11**, 6925–6934.
65 F. Baril-Robert, X. B. Li, M. J. Katz, A. R. Geisheimer, D. B. Leznoff and H. Patterson, *Inorg. Chem.*, 2011, **50**, 231–237.
66 C. Kappenstein, A. Ouali, M. Guerin, J. Cernak and J. Chomic, *Inorg. Chim. Acta*, 1988, **147**, 189–197.
67 L. Triscikova, J. Chomic, K. S. Abboud, J. H. Park, M. W. Meisel and J. Cernak, *Inorg. Chim. Acta*, 2004, **357**, 2763–2768.
68 A. Karadag, A. Aydin, S. Dede, S. Tekin, Y. Yanar, B. H. Cadirci, M. S. Soylu and O. Andac, *New J. Chem.*, 2015, **39**, 8136–8152.
69 J. Piromchom, N. Wannarit, C. Pakawatchai and S. Youngme, *Acta Crystallogr., Sect. C: Cryst. Struct. Commun.*, 2013, **69**, 1136–1139.
70 T. V. Popova and N. V. Aksenova, *Russ. J. Coord. Chem.*, 2003, **29**, 743–765.
71 C. C. L. McCrory, X. Ottenwaelder, T. D. P. Stack and C. E. D. Chidsey, *J. Phys. Chem. A*, 2007, **111**, 12641–12650.
72 G. A. Ardizzoia, S. Brenna, S. Durini and B. Therrien, *Polyhedron*, 2015, **90**, 214–220.
73 G. A. Ardizzoia, G. Colombo, B. Therrien and S. Brenna, *Eur. J. Inorg. Chem.*, 2019, **2019**, 1825–1831.
74 G. A. Ardizzoia, S. Brenna, S. Durini, B. Therrien and M. Veronelli, *Eur. J. Inorg. Chem.*, 2014, **2014**, 4310–4319.
75 M. D. Weber, C. Garino, G. Volpi, E. Casamassa, M. Milanesio, C. Barolo and R. D. Costa, *Dalton Trans.*, 2016, **45**, 8984–8993.
76 C. M. Álvarez, L. Álvarez-Miguel, R. García-Rodríguez, J. M. Martín-Álvarez and D. Miguel, *Eur. J. Inorg. Chem.*, 2015, **2015**, 4921–4934.
77 M. E. Bluhm, M. Ciesielski, H. Görls, O. Walter and M. Döring, *Inorg. Chem.*, 2003, **42**, 8878–8885.
78 Y. Chen, L. Li, Y. Cao, J. Wu, Q. Gao, Y. Li, H. Hu, W. Liu, Y. Liu, Z. Kang and J. Li, *CrystEngComm*, 2013, **15**, 2675–2681.
79 S. Priyanga, T. Khamrang, M. Velusamy, S. Karthi, B. Ashokkumar and R. Mayilmurugan, *Dalton Trans.*, 2019, **48**, 1489–1503.
80 N. Kundu, M. Maity, P. B. Chatterjee, S. J. Teat, A. Endo and M. Chaudhury, *J. Am. Chem. Soc.*, 2011, **133**, 20104–20107.
81 Y. Chen, L. Li, Z. Chen, Y. Liu, H. Hu, W. Chen, W. Liu, Y. Li, T. Lei, Y. Cao, Z. Kang, M. Lin and W. Li, *Inorg. Chem.*, 2012, **51**, 9705–9713.
82 A. Giordana, E. Priola, E. Bonometti, P. Benzi, L. Operti and E. Diana, *Polyhedron*, 2017, **138**, 239–248.
83 R. J. Roberts, D. Le and D. B. Leznoff, *Chem. Commun.*, 2015, **51**, 14299–14302.
84 K. H. Schmidt and A. Müller, *J. Mol. Struct.*, 1974, **22**, 343–352.
85 B. N. Cyvin, S. J. Cyvin, K. H. Schmidt, W. Wiegeler, A. Müller and J. Brunvoll, *J. Mol. Struct.*, 1976, **30**, 315–332.
86 K. Nakamoto, *Infrared and Raman Spectra of Inorganic and Coordination Compounds*, 2008, pp. 1–273.
87 A. Bromberg, S. Kimel and A. Ron, *Chem. Phys. Lett.*, 1977, **46**, 262–266.
88 E. Priola, G. Mahmoudi, J. Andreo and A. Frontera, *Chem. Commun.*, 2021, **57**, 7268–7271.
89 M. Frey and M. Ledésert, *Acta Crystallogr., Sect. B: Struct. Crystallogr. Cryst. Chem.*, 1971, **27**, 2119–2123.
90 P. T. T. Wong, *J. Chem. Phys.*, 1980, **72**, 6721–6725.
91 G. Gervasio and M. Marabello, *Acta Crystallogr., Sect. C: Cryst. Struct. Commun.*, 2007, **63**, m318–m320.
92 A. E. O'Connor, N. Mirzadeh, S. K. Bhargava, T. L. Easun, M. Schröder and A. J. Blake, *Chem. Commun.*, 2016, **52**, 6769–6772.
93 A. J. Blake, R. Donamaría, V. Lippolis, J. M. López-de-Luzuriaga, M. Monge, M. E. Olmos, A. Seal and J. A. Weinstein, *Inorg. Chem.*, 2019, **58**, 4954–4961.
94 R. J. Roberts, N. Bélanger-Desmarais, C. Reber and D. B. Leznoff, *Chem. Commun.*, 2014, **50**, 3148–3150.
95 C. H. Woodall, S. Fuertes, C. M. Beavers, L. E. Hatcher, A. Parlett, H. J. Shepherd, J. Christensen, S. J. Teat, M. Intissar, A. Rodrigue-Witchel, Y. Suffren, C. Reber, C. H. Hendon, D. Tiana, A. Walsh and P. R. Raithby, *Chem. – Eur. J.*, 2014, **20**, 16933–16942.
96 D. Paliwoda, P. Wawrzyniak and A. Katrusiak, *J. Phys. Chem. Lett.*, 2014, **5**, 2182–2188.
97 C. H. Woodall, J. Christensen, J. M. Skelton, L. E. Hatcher, A. Parlett, P. R. Raithby, A. Walsh, S. C. Parker, C. M. Beavers, S. J. Teat, M. Intissar, C. Reber and D. R. Allan, *IUCrJ*, 2016, **3**, 367–376.

98 V. Monteseguro, D. Errandonea, S. N. Achary, J. A. Sans, F. J. Manjón, S. Gallego-Parra and C. Popescu, *Inorg. Chem.*, 2019, **58**, 10665–10670.
99 J. Strasser, H. Yersin and H. H. Patterson, *Chem. Phys. Lett.*, 1998, **295**, 95–98.
100 P. Fischer, J. Mesot, B. Lucas, A. Ludi, H. Patterson and A. Hewat, *Inorg. Chem.*, 1997, **36**, 2791–2794.
101 D. M. Adams and P. A. Fletcher, *Spectrochim. Acta, Part A*, 1988, **44**, 437–443.
102 J. A. Rodríguez-Velamazán, L. Canadillas-Delgado, M. Castro, G. J. McIntyre and J. A. Real, *Acta Crystallogr., Sect. B: Struct. Sci., Cryst. Eng. Mater.*, 2014, **70**, 436–443.
103 G. Agustí, A. B. Gaspar, M. C. Muñoz and J. A. Real, *Inorg. Chem.*, 2007, **46**, 9646–9654.
104 L. Ould-Moussa, M. Castellà-Ventura, E. Kassab, O. Poizat, D. P. Strommen and J. R. Kincaid, *J. Raman Spectrosc.*, 2000, **31**, 377–390.
105 R. E. Wilde and T. K. K. Srinivasan, *J. Inorg. Nucl. Chem.*, 1974, **36**, 323–328.
106 B. M. Chadwick and S. G. Frankiss, *J. Mol. Struct.*, 1976, **31**, 1–9.
107 E. V. Boldyreva, *Acta Crystallogr., Sect. A: Found. Crystallogr.*, 2008, **64**, 218–231.
108 E. V. Boldyreva, *Cryst. Eng.*, 2003, **6**, 235–254.
109 E. Priola, A. Giordana, P. P. Mazzeo, G. Mahmoudi, R. M. Gomila, F. I. Zubkov, K. M. Pokazeev, K. S. Valchuk, A. Bacchi, E. Zangrando and A. Frontera, *Dalton Trans.*, 2021, DOI: 10.1039/D1DT02632A.
110 M. A. Omary and H. H. Patterson, *Inorg. Chem.*, 1998, **37**, 1060–1066.
111 P. Fischer, B. Lucas, M. A. Omary, C. L. Larochelle and H. H. Patterson, *J. Solid State Chem.*, 2002, **168**, 267–274.
112 P. Fischer, B. Lucas, H. H. Patterson and C. L. Larochelle, *Appl. Phys. A: Mater. Sci. Process.*, 2002, **74**, s1296–s1298.